Non-invasive monitoring of water infiltration in a silty clay loam soil using Spectral Induced Polarization

A. Ghorbani,[1,2] Ph. Cosenza,[1,2] S. Ruy,[3] C. Doussan,[3] and N. Florsch[1,2]

Received 13 April 2007; revised 13 February 2008; accepted 3 March 2008; published 1 August 2008.

[1] An experimental investigation was undertaken to study the ability of Spectral Induced Polarization (SIP) to monitor water infiltration in a silty clay loam soil. It was based on the coupled acquisition of tensiometer data and Spectral Induced Polarization (SIP) spectra (1.46 Hz to 12 kHz) during the infiltration event created by an artificial constant rainfall rate of about 15 mm/h. The approach, which was applied both in the field and in a soil column, confirms the existence of a significant phase drop in the high-frequency domain (typically greater than 1 kHz) during the first infiltration cycles. The interpretation of the tensiometer and SIP data show that this phase drop is correlated with the water filling of pores in the [30–85] μm diameter range. The phase drop is qualitatively and quantitatively interpreted as a Maxwell-Wagner effect associated with the electrical heterogeneity of the soil. It could correspond to the transition between two physical states. In the first state before the arrival of the wetting front, highly polarized and wet aggregates are embedded in an electrically isolating phase, i.e., air. In the second state after the arrival of the wetting front, structural pores between the aggregates are filled with a connected and conducting phase, i.e., water, leading macroscopically to a decrease in bulk soil polarizability. The experimental and theoretical results of this study suggest strongly that the SIP method can be used to monitor the water filling of structural or draining pores in the field. This original result requires validation in other sites.

Citation: Ghorbani, A., Ph. Cosenza, S. Ruy, C. Doussan, and N. Florsch (2008), Non-invasive monitoring of water infiltration in a silty clay loam soil using Spectral Induced Polarization, *Water Resour. Res.*, *44*, W08402, doi:10.1029/2007WR006114.

1. Introduction

[2] Both dielectric and electrical methods have been used for decades in soil science in order to quantify the changes in soil water content and soil salinity [e.g., *Smith-Rose*, 1933]. Dielectric methods, which measure the relative dielectric permittivity in the 10 MHz to 1 GHz frequency range, include (a) time domain reflectometry (TDR) probes [e.g., *Davis et al.*, 1977], capacitance sensors [e.g., *Tran Ngoc et al.*, 1972] and ground-penetrating radar [e.g., *Chanzy et al.*, 1996]. The electrical methods, which are often called DC (Direct Current) or low-frequency electrical techniques, measure the electrical conductivity (EC) in the few Hz to 10 kHz frequency range. Example methods include (1) low-cost electric resistance methods (gypsum block for matric potential measurements) [e.g., *Bouyoucos and Mick*, 1940] and (2) four-electrode methods used both in the laboratory and the field [e.g., *Tabbagh et al.*, 2000].

[3] In electrical methods, the measured EC is an in-phase conductivity and is associated with the in-phase conduction of the reference electric current. However, the measured electrical impedance is generally a complex quantity with a corresponding in-phase and quadrature component [e.g., *Keller and Frischknecht*, 1982; *Ward*, 1990]. In the frequency domain, this quadrature conduction is related to a phase shift between the measured voltage and the applied alternative current. The quadrature conduction at low frequencies (typically from 10 mHz up to 10 kHz) is referred to in geophysics as induced polarization (IP), complex electrical conductivity or complex resistivity. The method used to measure the spectra of these complex quantities is called Spectral Induced Polarization (SIP).

[4] Initially, the IP method was developed for detecting small concentrations of disseminated mineralization in base metal exploration [e.g., *Marshall and Madden*, 1959; *Van Voorhis et al.*, 1973]. However, recently, attention has focused on IP in rocks and soils as a means of determining surface properties indirectly (cation exchange capacity and specific surface area) [*Vinegar and Waxman*, 1984; *Olhoeft*, 1985; *Börner and Schön*, 1991; *Slater and Glaser*, 2003; *Lesmes and Morgan*, 2001; *Slater et al.*, 2005] and hydraulic conductivity [*Börner et al.*, 1996; *Lima and Niwas*, 2000; *Comas and Slater*, 2004; *Binley et al.*, 2005; *Tong et al.*, 2006]. The experimental investigations of *Titov et al.* [2002] and *Scott and Barker* [2003] showed that pore-throat diameters and pore geometry in water-saturated geomaterials contribute significantly to both in-phase and out-of-phase conduction at low frequencies. IP measurements performed on unsaturated sands submitted to various infiltration-drainage cycles have shown that IP parameters exhibit a complex saturation dependence and are a function of saturation range and saturation history [*Ulrich and Slater*,

[1]UPMC, University of Paris, Sisyphe, Paris, France.
[2]CNRS, Sisyphe, Paris, France.
[3]INRA-UMR Climat, Sol Environnement, Avignon, France.

0043-1397/08/2007WR006114$09.00

2004]. *Titov et al.* [2004] confirmed the previous results and proposed an IP model for unsaturated sands. This model is able to detect the critical water saturation, which corresponds to the change in pore-water geometry from bulk water to an adsorbed film existing on the quartz grains. However, not all of the aforementioned experimental investigations examined natural soils with an associated broad distribution of particles, pores and aggregate sizes.

[5] In summary, although the IP method has become increasingly popular in environmental and groundwater investigations [e.g., *Binley and Kemna*, 2005; *Börner*, 2006], its full potential has yet to be realized in hydrological sciences, especially in topics related to flow and transport in partially saturated soils.

[6] Indeed, among these topics, the noninvasive characterization of water infiltration in unsaturated soils is still an active field of research [e.g., *Dingman*, 2002]. Although the DC electrical method has been reported to be able to monitor flows in the vadose zone [e.g., *Daily et al.*, 1992; *Hagrey and Michaelsen*, 1999; *Zhou et al.*, 2001], the SIP method has never been used for this purpose. The aim of this work was to address experimentally the capabilities of the SIP method for characterizing vertical flows in the vadose zone during an infiltration test.

[7] Our approach is based on both field and laboratory experiments that couple SIP measurements and hydraulic measurements as performed in a natural agricultural soil.

[8] First, the IP (and hence SIP) method and the underlying physical mechanisms are briefly reviewed and the various IP parameters are discussed. The field and laboratory experiments are presented in the second and the third part of the paper, respectively. Finally, the results are discussed in the fourth part.

2. Induced Polarization: Theoretical and Phenomenological Aspects

2.1. Complex Electrical Properties

[9] The concepts of complex conductivity and complex resistivity are directly related to Maxwell's postulate: the total electric current density $\mathbf{J_t}$ is the sum of the conduction current density $\mathbf{J_c}$ and the displacement current density $\mathbf{J_d}$, which are both defined by the following constitutive equations for time harmonic fields [e.g., *Guéguen and Palciauskas*, 1994]:

$$\boldsymbol{J_c} = \sigma \boldsymbol{E} = \frac{1}{\rho}\boldsymbol{E} \tag{1}$$

$$J_d = \frac{\partial D}{\partial \mathrm{t}} = \mathrm{i}\omega\kappa^*\varepsilon_0 E \tag{2}$$

where σ is electrical conductivity, ρ is electrical resistivity, $\boldsymbol{E}$ is applied electric field, $\boldsymbol{D}$ is the electric displacement, t is time, i is $\sqrt{-1}$, ε_0 is the permittivity of the vacuum and κ^* is the complex relative permittivity. Equation (1) is referred to as Ohm's law.

[10] Consequently, by using equations (1) and (2), the total current density can be expressed as

$$\boldsymbol{J_t} = \boldsymbol{J_c} + \boldsymbol{J_d} = (\sigma + \mathrm{i}\omega\kappa^*\varepsilon_0)\boldsymbol{E} = \sigma^*\boldsymbol{E} = \frac{1}{\rho^*}\boldsymbol{E} \tag{3}$$

where σ^* and ρ^* are the complex conductivity and the complex resistivity, respectively. By comparison with (2), equation (3) can be rewritten in order to introduce an effective complex relative permittivity κ_{eff}^*:

$$\boldsymbol{J}_t = \mathrm{i}\omega\kappa_{eff}^*\varepsilon_0\boldsymbol{E} \tag{4}$$

[11] The complex electrical properties, σ^*, ρ^* and κ_{eff}^* are linked with each other by the following relationships:

$$\sigma^* = \frac{1}{\rho^*} = \mathrm{i}\omega\varepsilon_0\kappa_{eff}^* \tag{5}$$

[12] Generally, these complex properties measured in Earth materials are frequency dependent, i.e., they show an electrical dispersion. They can be split into two parts, i.e., a real component and an imaginary (or in-phase and quadrature) component. They can also be expressed in polar form as a magnitude and a phase. For instance, complex resistivity can be written as:

$$\rho^* = \rho' + \mathrm{i}\rho'' = |\rho^*|\exp(\mathrm{i}\phi) \tag{6}$$

where ρ', ρ'' and $|\rho^*|$ are the real part, the imaginary and the resistivity amplitude of ρ^* respectively, and ϕ is the phase of ρ^* that can be also written as follows:

$$\phi = \tan^{-1}\left(\frac{\rho''}{\rho'}\right) \approx \frac{\rho''}{\rho'}(\textit{typically if } |\phi| < 100 \textit{ mrads}) \tag{7}$$

or from equation (5):

$$\phi = -\tan^{-1}\left(\frac{\kappa'_{eff}}{\kappa''_{eff}}\right) = -\tan^{-1}\left(\frac{\sigma''}{\sigma'}\right) \approx -\frac{\sigma''}{\sigma'}(\textit{typically if } |\phi| < 100 \textit{ mrads}) \tag{8}$$

where κ'_{eff} and κ''_{eff} are the real and imaginary parts of the complex relative permittivity κ_{eff}^*, respectively. Parameters σ' and σ'' are the real and imaginary parts of the complex conductivity σ^*, respectively.

2.2. Polarization Mechanisms and Models in the Low Frequency Range

[13] The purpose of this section is not to establish an exhaustive summary of the experimental and theoretical works devoted to polarization mechanisms but to give the main physical concepts widely used. For a comprehensive review of such works, the reader is referred to *Chelidze and Guéguen* [1999], *Lesmes and Morgan* [2001], *Santamarina* [2001] and references therein.

[14] In general, any mechanism, which restrains the relative displacement of charges, can be considered as a polarization mechanism (charge displacement without restriction renders conductivity) [e.g., *Santamarina*, 2001]. This leads to an accumulation of negative charges, (i.e., an electrical pole) on one side of the medium and positive charges (i.e., another pole) on the opposite side. In effect, the medium becomes polarized.

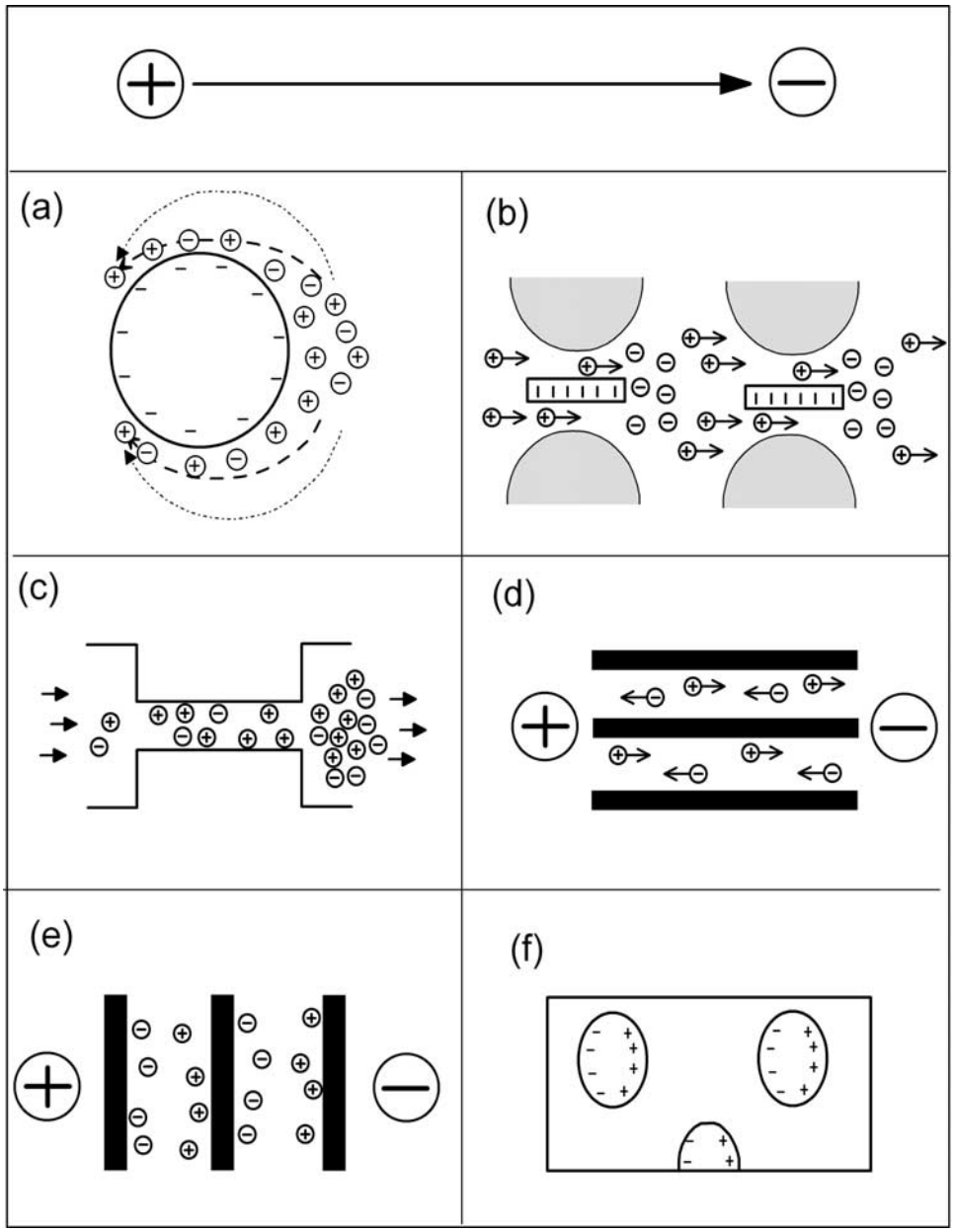

Figure 1. Electrical polarization mechanisms (modified from *Santamarina* [2001] and *Titov et al.* [2004]). (a) Electrical Double Layer (EDL) polarization. The figure illustrates excess and deficiency in ion concentration around a polarized particle. Dotted line indicates the local diffusion flows of both cations and anions; dashed line gives the local diffusion flows near the solid surface. (b) Membrane polarization. Clay particles at pore throats constitute ion-selective zones. The EDL is not drawn for clarity. (c) Polarization associated with pore throats. Pore throats with corresponding EDL constitute ion-selective zones. The EDL is not drawn for clarity. (d) No interfacial polarization: the layered medium is parallel to the electric field. (e) Maxwell (interfacial) polarization: the layered medium is perpendicular to the electric field. (f) Wagner (interfacial) polarization. Dielectric host with conductive inclusions.

[15] In the low frequency ranges (typically from 10 mHz up to 10 kHz), the restrained relative displacement of charges in geomaterials may have two origins.

[16] The first origin is electrochemical and it is related to the existence of an electrical double layer (EDL) at the interface between solid and liquid phases. The EDL results from usually negative electrical surface charges existing in the solid particles and appears at the solid-liquid interface, as an oppositely charged ion atmosphere. In the EDL, the average concentration of cations (in the case of negatively charged surfaces) is larger than that of anions. There are two clearly distinguishable groups of electrochemical mechanisms and models. In the first group, models have been introduced to account for the dielectric response of dilute suspensions of spherical particles from Colloid Science [e.g., *Lyklema*, 1995] (Figure 1a). In the second, the Marshall-Madden model has been especially proposed for rocks with a dispersed clay fraction [e.g., *Marshall and*

Table 1. Main Mean (n = 2) Characteristics of the Soil for the 30 cm Upper Layer[a]

% Clay, (g g^{-1})	% Silt, (g g^{-1})	CEC, (cmol kg^{-1})	Ca^{++}, (cmol kg^{-1})	Na^{+}, (cmol kg^{-1})	Mg^{++}, (cmol kg^{-1})	K^{+}, (cmol kg^{-1})	C_{org}, (g kg^{-1})
34.5	54.0	11.9	39.5	0.72	1.52	0.5	14.4

[a]Corg = content of organic carbon.

Madden, 1959]. In this model, rock is considered as a serial connection of active (ion-selective) and passive (nonselective) zones. Clay minerals coating the quartz grains or located in pore throats [*Ward*, 1990] and pore throats themselves associated with an EDL [*Scott and Barker*, 2003; *Titov et al.*, 2002] are selective zones (Figures 1b and 1c). The first case in which clay minerals play a significant role is often called "membrane polarization" (Figure 1b). These active and passive zones have different transport Hittorf numbers [e.g., *Revil et al.*, 1998], which produces local concentration gradients under applied external voltage. These concentration gradients induce local solute flows and hence an additional electrical current leading to the phase shift and the frequency dependency of the resistivity observed in IP measurements [*Titov et al.*, 2002].

[17] The second main origin of low-frequency polarization in Earth materials is geometrical and interfacial (GI). The GI or spatial polarization mechanism results from differences in conductivity and polarizability among components in a mixture, producing charge accumulation at the interface. The first calculation related to GI polarization was made by *Maxwell* [1891], who considered layered materials (Figure 1d and Figure 1e). As *Wagner* [1924] solved the complex permittivity of a dilute suspension of conductive spheres (Figure 1f), interfacial polarization is also known as the Maxwell-Wagner effect. This mechanism, which can be seen as a bulk effect, has a pure macroscopic definition and does not require any comprehensive understanding of the physical process of charge accumulation at the molecular level.

[18] The most popular formulation for modeling the Maxwell-Wagner effect in Earth Sciences is the Maxwell-Wagner-Hanai-Bruggeman (MWHB) equation [e.g., *Chelidze and Guéguen*, 1999; *Lesmes and Morgan*, 2001; *Cosenza et al.*, 2003], which corresponds to a differential effective medium (DEM) theory. Consider a mixture of two components: spheroidal inclusions with an effective complex permittivity κ_i are embedded in a matrix characterized by an effective complex permittivity κ_{m}. The effective complex permittivity of the mixture κ_{mix} is given by the MWHB equation:

$$\frac{\kappa_i - \kappa_{\mathrm{mix}}}{\kappa_i - \kappa_{\mathrm{m}}}\left(\frac{\kappa_{\mathrm{m}}}{\kappa_{\mathrm{mix}}}\right)^{1/\mathrm{m}} = 1 - d_i \tag{9}$$

where d_i is the volume fraction of spheroidal inclusions, m is a particle shape factor related to the eccentricity of the spheroidal inclusions and is also called the "cementation exponent". Obviously, from equation (5), the MWHB equation (9) can also be expressed in terms of complex conductivity or complex resistivity. Thus *Samstag and Morgan* [1991] used a similar equation expressed in terms of complex conductivity to model the IP of saturated shaly sands.

[19] The GI and electrochemical models are not incompatible since they operate at different scales. For instance, *Lesmes and Morgan* [2001] proposed a granular model for the electrical properties of saturated sedimentary rocks that combines both approaches. On the basis of their model, the MWHB equation was considered as a mixture formula in which the electromagnetic properties of components, especially the clay fraction, are governed by microscopic and physico-chemical laws.

3. Field Experiments

3.1. Soil, Experimental Setup and Procedure

[20] Field experiments were undertaken on a silty clay loam soil of an agricultural INRA field site located near Avignon in Southern France. The A horizon (0–60 cm) is made of a tilled layer (0–30 cm) overlapping an undisturbed layer with centimetric (0–15 cm layer) to decimetric (15–30 cm layer) polyhedric clods. The main characteristics are given in Table 1.

[21] A square plot of 0.99 × 0.99 m was established (Figure 2). A trench about 30 cm deep was dug around the perimeter of the plot. A PVC wall was placed in the trench against the inside wall of the plot, except on one side so that possible runoff water could drain away (Figure 2). Twenty-four automatic pressure transducers connected to micro-tensiometers (2.2 mm in diameter, SDEC France) were placed in the plot 20 cm and 40 cm apart at depths of 8 cm and 13 cm (Figure 2). The 24 tensiometers were grouped into 4 subgroups by 4 switching boxes connected to a data logger (CR10X, Campbell Scientific).

[22] SIP measurements were carried out with the SIP-FUCHS II device (Radic Research) which measures complex resistivity over 7 decades of frequency (1.4 mHz up to 12 kHz) with 4 electrodes. It consists of two remote units that record current I injected by two electrodes A and B and voltage U signals measured between two electrodes M and N (Figure 2). The apparent complex resistivity ρ^* is estimated by:

$$\rho^*(\omega) = 2\pi a \frac{U}{I} = |\rho^*(\omega)| e^{i\phi(\omega)} \tag{10}$$

where ($i^2 = -1$); a is the electrode separation; $|\rho^*(\omega)|$ and ϕ (ω) are the resistivity amplitude and the phase respectively. They are a priori a function of the angular frequency ω. Equation (10) gives an "apparent" value of the resistivity, which is the resistivity of a homogeneous ground that will give the same impedance for the same electrode array [e.g., *Parasnis*, 1997].

[23] To measure the whole spectrum of both parameters, $|\rho^*(\omega)|$ and $\phi(\omega)$, the SIP FUCHS-II apparatus starts with the highest frequency, 12 kHz, and the N other decreasing frequencies are obtained by the following division: 12 kHz/

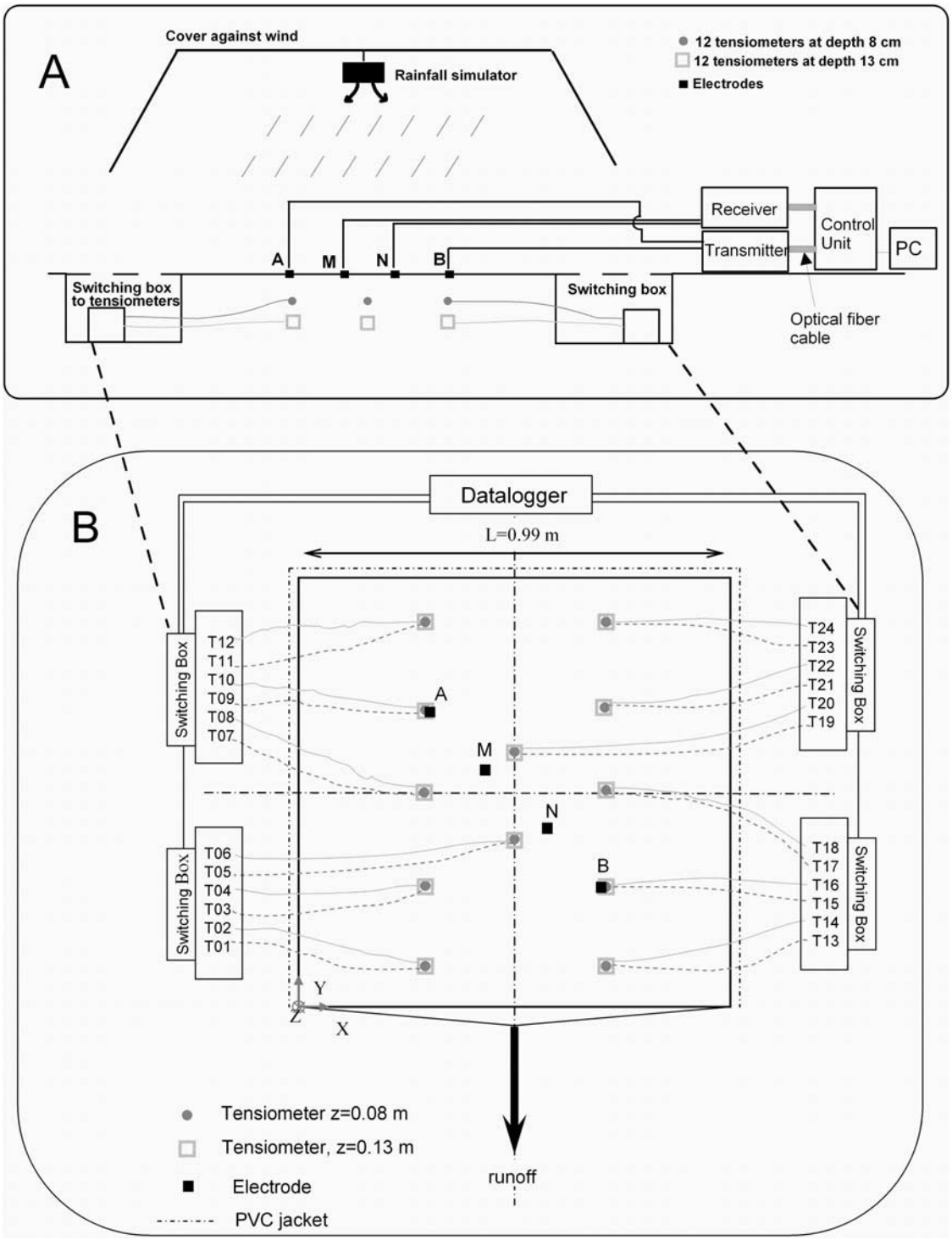

Figure 2. Schematic view of the field experimental setup. (A) Cross-section, (B) top view.

2^N. Optical fibers are used in order to minimize electromagnetic cross-couplings between the transmitter and the receiver and to ensure a system-wide synchronization. The measured data are transferred to the base unit, where the impedance amplitude and the phase shift are determined. The SIP FUCHS-II is connected to a computer in order to record the data and to display the results in real time.

[24] To minimize the so-called ''electrode polarization'' associated with electrochemical reactions occurring at the electrode-sample boundary [e.g., *Chelidze et al.*, 1999], the A and B current electrodes were $Cu/CuSO_4$ electrodes whereas the M and N electrodes were $Pb/PbCl_2$ electrodes [e.g., *Petiau*, 2000].

[25] In order to estimate the phase error associated solely with the instrument, the phase was measured with pure resistors [ranging from 15–10,000 Ohm] and with different configurations of BNC cables (maximum length equal to 1 m). The maximum phase error measured for 15 Ohm at

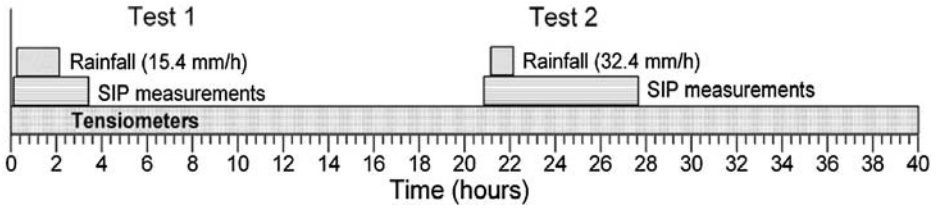

Figure 3. Schematic view of the experimental procedure.

12 kHz is less than 2.5 mrads. This error decreases drastically and nonlinearly with frequency down to 0.4 mrad at 1.5 kHz. It becomes negligible (less than 0.1 mrad) when frequency is lower than 100 Hz. Within the same impedance range, the absolute impedance error is less than 0.1%.

[26] The electrodes were vertically installed in the plot. A Wenner array configuration was used with the electrodes 20 cm apart. In this array, the four electrodes are collinear and the intervals between adjacent electrodes are equal (Figure 2). If a homogeneous soil is being studied, the depth of investigation of such an array, for which the sensitivity to vertical changes in electrical properties is maximum, is about 10.4 cm, i.e., AB $\times$ 0.519 [e.g., *Edwards*, 1977], which is between the two depths of the tensiometers. Nevertheless, it should be borne in mind that: (1) the value of 10.4 cm is an order of magnitude used for planning the field experiment since the studied system (water front displacement in a dry soil) is intrinsically heterogeneous; (2) the measured amplitude and phase are complex averages of these parameters over the depth of investigation, so they are not local measurements, as is the case for tensiometer measurements.

[27] Water infiltration in the soil was achieved by a rainfall simulator (Institut de Recherche pour le Développement-IRD model) which provided a constant rainfall rate in the range of 10–100 mm·h^{-1}. In order to check the impact of the electrical noise generated by the rainfall simulator, low-frequency measurements were undertaken before and after switching on the rainfall simulator. No significant change was measured between these two states.

[28] Fresh water taken from the water table located at the site was used as the wetting fluid for all experiments. Its conductivity was equal to 930 μS/cm at 20°C.

[29] The field experiment was conducted in two main phases (Figure 3). First, an infiltration test (Test 1) with a rainfall rate of 15.4 mm/h was performed for about 2 h. Before, during and after this rainfall event, an electrical resistivity spectrum between 1.46 Hz to 12 kHz was measured every 2 min. As the soil was initially in a dry state (initial volumetric water content of 0.240 m^3·m^{-3}, which corresponds to a matric potential lower than -10 m), tensiometers were inserted into the soil only 30 min before the beginning of the rainfall simulation in order to avoid their desaturation. It follows that the first pressure measurements are not representative of the soil water matric potential as the tensiometers were not in equilibrium with the soil water. Representative measurements are obtained only after the arrival of the wetting front at the depth of insertion. In the second phase (Test 2 in Figure 3) one day later, a new infiltration test with a higher rainfall rate of 32.4 mm/h was carried out for about 1 h. The soil was wet (matric potential about −0.35 m which corresponds to a water content of 0.350 m^3·m^{-3}). Electrical resistivity spectra were measured again with the same procedure as in Test 1, for the frequency range: 0.732 Hz to 12 kHz. During both phases, the soil water matric potentials were recorded with a 10-s sampling interval.

3.2. Results

[30] During Test 1, no surface ponding occurred at any time. The rate of infiltration into the soil was equal to the rainfall rate. The matric potential measurements located at the same depth, as indicated in Figure 4 for six tensiometers, showed significant differences in terms of amplitude and temporal dynamics. This spatial variability is also illustrated in Figure 5 where the times corresponding to the arrival of a wetting front (i.e., fast increase of the matric potential, becoming less negative) are plotted. Both figures confirm an infiltration process associated with a significant spatial heterogeneity of the structured soil studied.

[31] To compare these results with geophysical measurements in order to obtain average values of SIP parameters over about 10 cm, tensiometer values were averaged for the two groups of 12 tensiometers located at the two depths, 8 cm and 13 cm (Figure 6). The average value at 13 cm clearly shows that, during water infiltration, the initial and rapid increase of the matric potential (at 22 min) was stopped at about 50 min (hereafter referred to as t_d), after

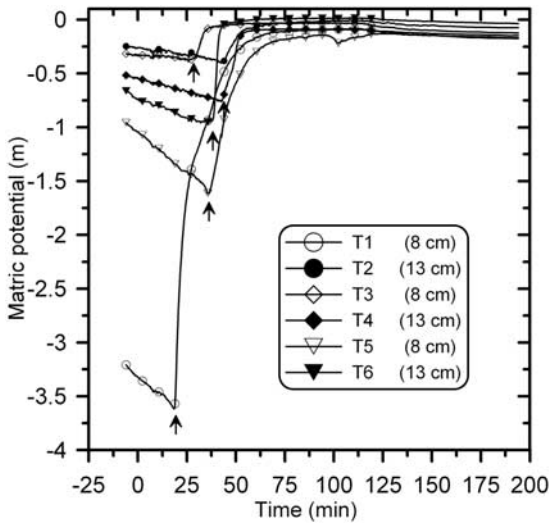

Figure 4. Matric potentials measured in 6 tensiometers (T1 to T6) versus time during Test 1. Time 0 corresponds to the beginning of the rainfall event of Test 1. The arrow indicates the arrival time of the wetting front at the tensiometer.

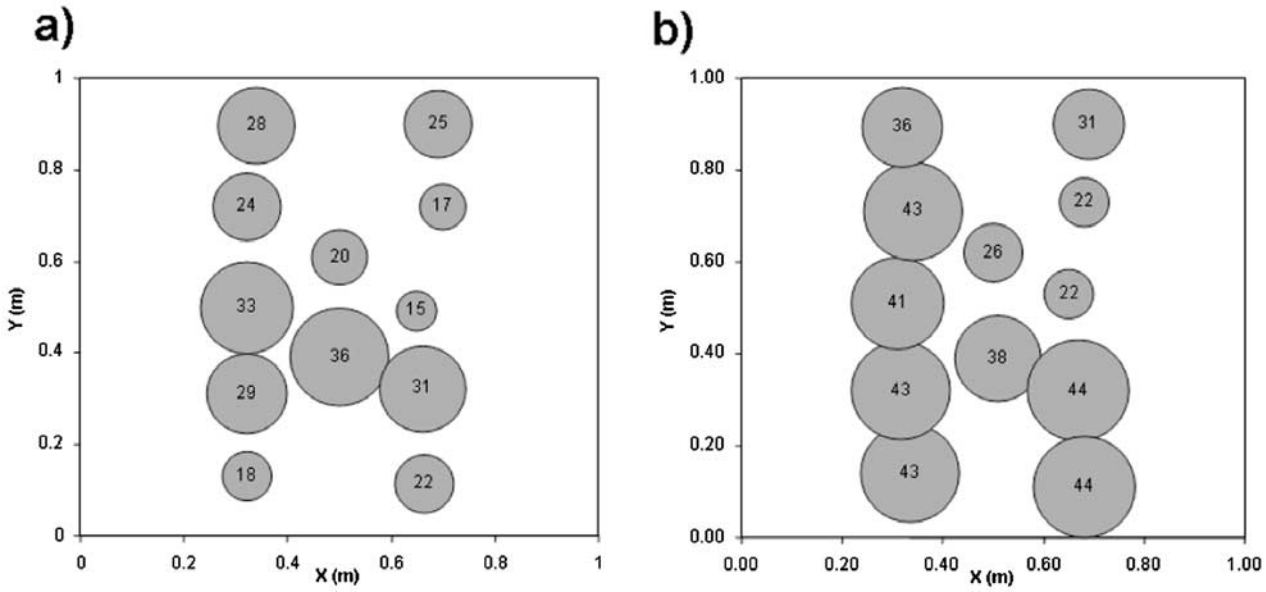

Figure 5. Arrival time in min for the wetting front observed for the 12 tensiometers located 8 cm deep (6a) and 13 cm deep (6b).

which the matric potential evolved more slowly. The time of 22 min (respectively 50 min) is interpreted as the average time for the wetting front to reach the depth of 13 cm (resp. as the average time to reach the steady state).

[32] Both components (phase and resistivity amplitude) of the complex resistivity spectrum versus time measured during Test 1 are given in Figure 7. The resistivity amplitude decreased during water infiltration and increased slowly when rainfall was stopped (Figure 7). The good sensitivity of resistivity amplitude to soil water content changes is already known: resistivity is a decreasing function of soil water content [e.g., *Rhoades et al.*, 1976]. Moreover, resistivity amplitude measurements show a very weak frequency dependence: the observed resistivity spectra were relatively flat.

[33] In comparison with amplitude, phase displayed a more complex behavior (Figure 7). Early during water infiltration, the phase angle increased slowly but significantly as the water content increased in the first centimeters of the soil. However, at time t_d (see arrow in Figure 7), the phase measured in the high frequency domain had dropped significantly with a higher level of noise. This rapid drop, which was not observed in the lower part of the frequency range, is related to the arrival of the wetting front in a zone where the sensitivity of the electrical parameters is maximal. Since this drop mainly concerns the phase measurements at time t_d and is enhanced in the higher part of the frequency range, a GI polarization mechanism was suspected to occur during the wetting front diffusion. This assumption will be discussed on the basis of results provided by a laboratory investigation and a subsequent model, both of which are presented in the last section.

[34] During infiltration, the phase continued to decrease slowly with a significant level of noise, likely related to the heterogeneity of the soil and the associated water movement. When the rainfall stopped, the phase returned almost to the initial level existing before the phase drop, and thereafter decreased slowly during the drainage phase. It should be noted that this phase reversibility was not associated with a hydraulic reversible behavior, as indicated in Figure 6.

[35] However, although a small Wenner array (electrode spacing equal to 20 cm) was used, one may wonder if the observed phase evolution would be related to an electromagnetic coupling due to the inductive response of the soil. This inductive response is caused by the electromagnetic alternating fields generated in situ by the device (grounded cables). In order to evaluate the EM coupling in our

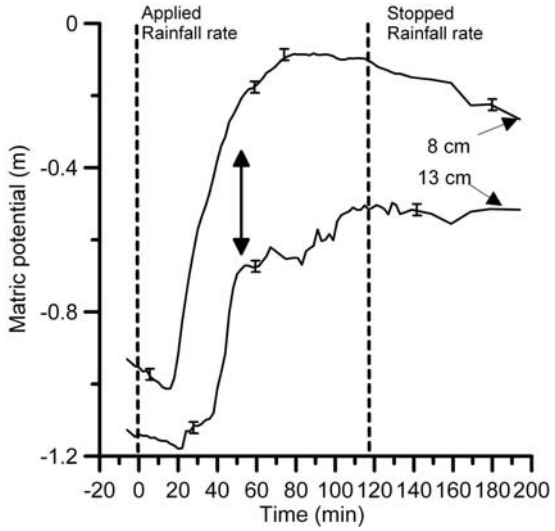

Figure 6. Mean matric potential at two depths (8 cm and 13 cm) versus time (Test 1). The beginning and the end of rainfall application are also shown. The arrow indicates a characteristic event which is compared to SIP measurements (see Figures 7 and 8). Typical error bars are also given.

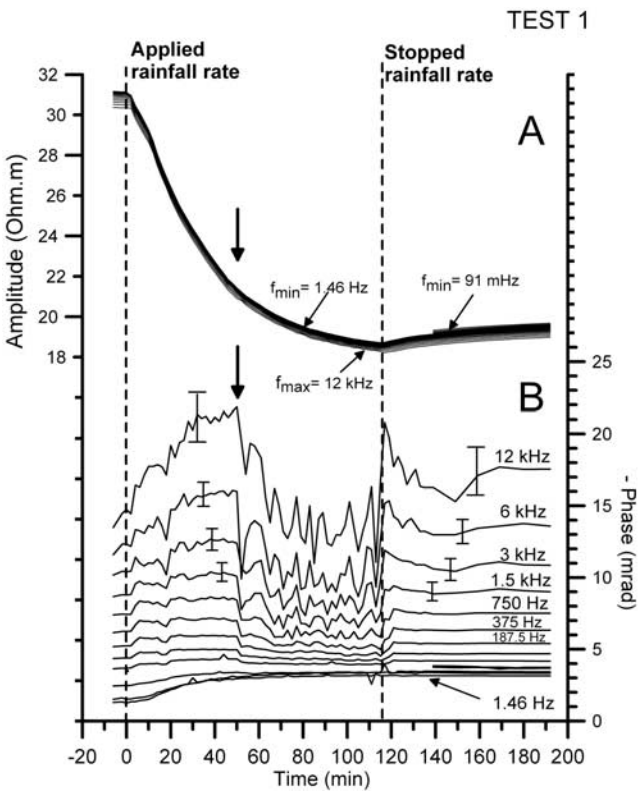

Figure 7. (A) Resistivity amplitude spectra versus time (Test 1). The beginning and the end of rainfall application are indicated by dashed lines. Note that at about time 145 min, a larger spectrum (from 91 mHz up to 12 kHz) was measured. (B) Phase spectra versus time (Test 1). The beginning and the end of rainfall application are also given. For clarity, the spectra below 187.5 Hz are not numbered. Typical error bars are also given. The phase drop indicated by an arrow is related to the average time for the wetting front to reach a steady state (see Figure 6). By convention the IP/capacitive effect is plotted as negative phase (i.e., $-$phase, $-\phi$).

experiment, the 1D forward modeling code, CR1Dmod, constructed by *Ingeman-Nielsen and Baumgartner* [2006] was used. The EM coupling was estimated by considering (1) a soil impedance range (15–40 Ohm) that corresponds to the impedance range measured in the field (2) a soil chargeability equal to zero (no soil polarization) in order to isolate the sole impact of the EM coupling and (3) an electrode spacing of 20 cm for a Wenner array and a length of the cables equal to 2 m. The CR1Dmod code evaluates a maximum phase of 3.5 mrad at 12 kHz that is lower than the amplitude of the measured phase drop ($\sim$10 mrad) at the same frequency. Moreover, an EM coupling associated with a monotonic decrease of the soil resistivity in the first dozen centimeters cannot induce a non monotonic change in the phase angle. In order to induce such a non monotone change with time, it is necessary to invoke a significant change in the soil polarizability during the infiltration.

[36] The results of Test 1 are also displayed in Figure 8 in terms of real conductivity σ' and the imaginary conductivity σ''. In the high frequency range, the transient evolution of the imaginary conductivity, which is primarily associated with polarization mechanisms, confirmed the transient evolution of the phase angle observed in Figure 7.

[37] Concerning Test 2, the matric potential prior to infiltration (Figure 9) was higher compared to Test 1 before the application of the rainfall rate. One-day drainage, redistribution and evaporation did not restore the initial soil-water state that existed before Test 1. A small amount of ponding was observed during Test 2. The resistivity spectra shown in Figure 10 were still sensitive to water content changes induced by water infiltration. The phase values were lower than those obtained during Test 1 (Figure 10). Moreover, contrary to Test 1, the phase spectra did not show any significant correlations with the transient matric potential variation given in Figure 9. Indeed, the phase drop observed during Test 1 was not detected during Test 2. This physical phenomenon is consequently related to a dry soil and possibly to a characteristic size of air-filled pores, above which the phase drop would not exist. This aspect will be discussed hereafter.

[38] The results of Test 2 are also expressed in terms of real conductivity σ' and imaginary conductivity σ'' in Figure 11. The transient evolution of σ' and σ'' confirm the transient evolution of the amplitude and the phase angle given in Figure 10.

[39] In summary, the results of this field experiment confirm the practical interest in using resistivity measurements to monitor soil water content but also demonstrate a surprising phase drop occurring during water infiltration in a dry soil. This peculiar pattern associated with phase

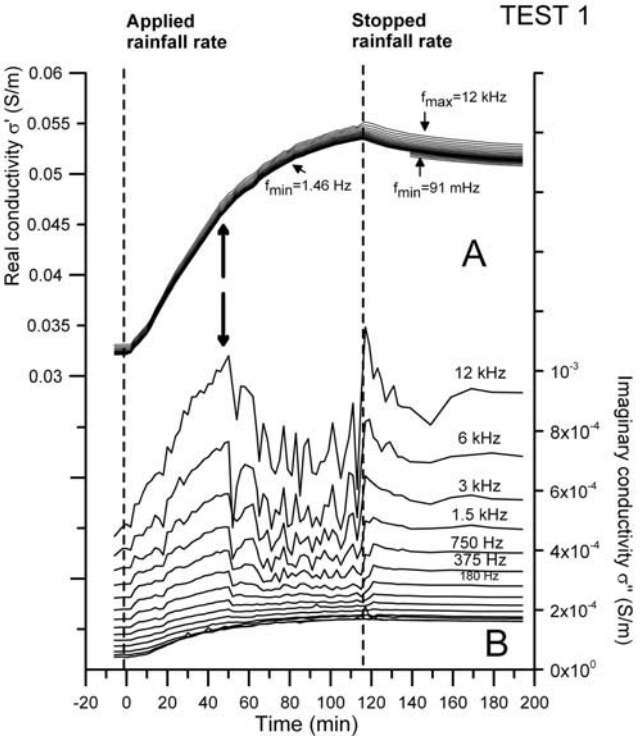

Figure 8. (A) Real conductivity spectra versus time (Test 1). (B) Imaginary conductivity spectra versus time (Test 1). The arrows are related to the average time for the wetting front to reach a steady state (see Figure 6).

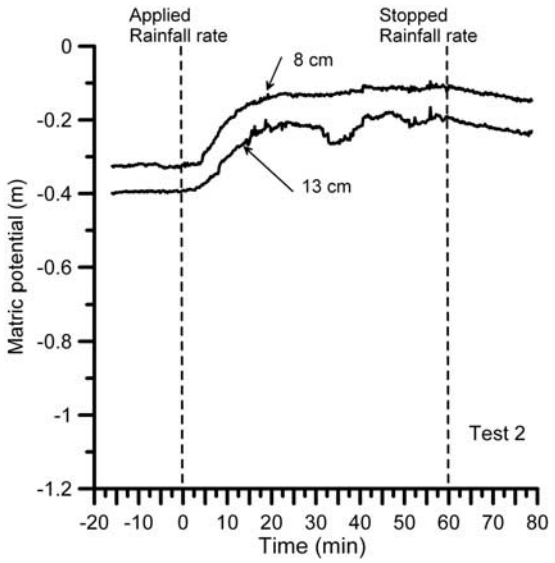

Figure 9. Mean matric potential at two depths (8 cm and 13 cm) versus time (Test 2). The beginning and the end of rainfall application are also given.

measurements has not observed in the literature to date and requires further experimental and theoretical work.

4. Column Experiments

4.1. Objective, Experimental Set-up and Procedure

[40] The objectives of this laboratory study were: (1) experimental confirmation of the phase drop measured in the field; (2) characterization in controlled conditions in order to substantiate a physical mechanism.

[41] The laboratory PVC column (Figure 12) was 280 mm high, had a 150 mm internal diameter and was filled with undisturbed core soil from the field experiment. Soil sampling was carried out carefully in order to obtain an undisturbed and representative soil sample in a dry state. The first 15 cm layer of the column was cloddy whereas the bottom part of the soil core was more massive. The column contained 10 microtensiometer ports located at depths given in Figure 12.

[42] The infiltration events were simulated by a rainfall simulator which was calibrated to provide a rainfall rate similar to that applied during the field experiments (i.e., 15 mm/h). The simulator area was close to that of the column in order to constrain the wetting profile to one dimension. The base of the column was not sealed in order to maintain a drained condition. The drainage water was weighed and its electrical conductivity was measured. The electrical conductivity of the infiltration water used for the experiment was 660 μS cm^{-1}.

[43] A laboratory complex resistivity system (1253 Gain-Phase analyzer Solartron Schlumberger) was used for electrical data acquisition. Four $Cu/CuSO_4$ electrodes were positioned in a horizontal plane located at 7 cm depth (Figure 12) where the soil structure was the most similar to that in the field. This electrode configuration offers two advantages. First, it makes it possible to test a very different configuration compared to that used in the field, i.e., the sensitivity of the geometric electrode array compared to the main direction of the water infiltration can be estimated. Second, its maximum sensitivity is in the electrode plane, i.e., the influence of the physical processes located at the top and the bottom of the column is minimized. Three high frequencies were considered: 93.5 Hz, 187 Hz, and 1.5 kHz in order to speed up the acquisition process with a high rate of sampling. Note that all three frequencies were also used by the SIP FUCHS-II field device. Moreover, in this laboratory configuration, the apparent complex resistivity is not given by equation (10): a new geometric factor, i.e., the 2 πa term in equation (10), had to be calculated. This factor related to the electrode configuration was quantified numerically by solving the Laplace equation with a finite difference scheme.

[44] In order to estimate the phase error associated with the instrument, the phase was measured with pure resistors [ranging from 10–10,000 Ohm] and with different configurations of BNC cables (maximum length equal to 1 m). The maximum phase error measured for 10 Ohm at 1.5 kHz was less than 2 mrad. Within the same impedance range, the absolute impedance error was less than 0.1 %. Moreover, in order to estimate the errors related to the contact resistance and the EM coupling associated with the wiring configura-

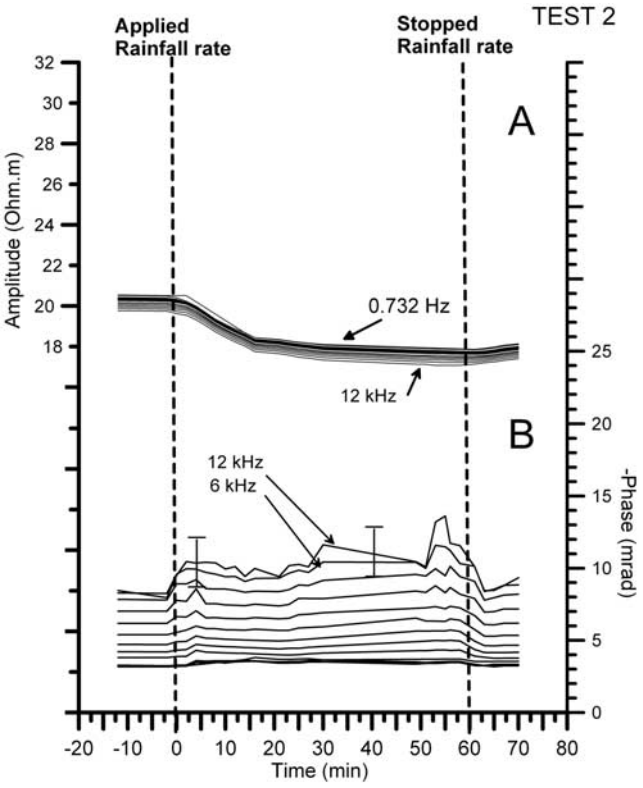

Figure 10. (A) Resistivity amplitude spectra versus time (Test 2). The beginning and the end of rainfall application are also indicated by dashed lines. For comparison, the same scale of amplitude used in Figure 7 has been used. (B) Phase spectra versus time (Test 2). The beginning and the end of rainfall application are also given. For clarity, not all the spectra are numbered. For comparison, the same scale of phase used in Figure 7 has been used. Typical error bars are also given. By convention the IP/capacitive effect is plotted as negative phase (i.e., -phase, $-\phi$).

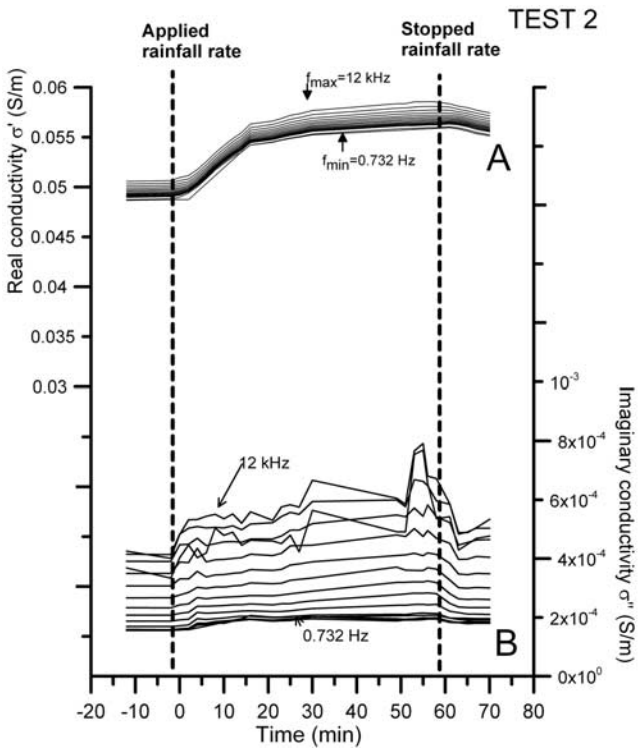

Figure 11. (A) Real conductivity spectra versus time (Test 2). (B) Imaginary conductivity spectra versus time (Test 2).

tion, an additional test with different electrolytic solutions was performed on a PVC column with geometry close to that of the soil column: it was 300 mm high an had a 190 mm internal diameter. In comparison with the soil column described previously, we used the same electrodes (in the same configuration) and the same laboratory complex resistivity system. The resistivity values of the electrolytic solutions were equal to 19.5 Ohm (514 μS/cm) and 1.4 Ohm·m (7100 μS/cm i.e., salt water). The measurements performed in over the frequency 10 Hz–1.5 kHz show a maximum positive error at 1.5 kHz equal to 6.9 mrads and 19.6 mrads for the water resistivities values of 19.5 Ohm·m and 1.4 Ohm·m, respectively (Figure 13): this error decreased significantly with the water resistivity. The value of 6.9 mrad is likely an upper bound of the experimental error since the range of 20–200 Ohm m is expected for the electrical resistivity of a clay loam soil.

[45] The laboratory experiment was conducted in two cycles (Figure 14). Each cycle consisted in an infiltration step by application of rainfall and a subsequent free drainage step with no applied rainfall. During both infiltration and drainage cycles, the matric potentials and the SIP parameters were recorded with a 2-min sampling interval.

4.2. Results

[46] Figures 15 and 16 show the matric potential variation during the first infiltration-drainage cycle. The results confirm that the water flow is vertical, one-dimensional and homogeneous at least until a depth of about 10 cm (Figure 15). On the other hand, the matric potential readings in the lower part of the column (Figure 16) strongly suggest that the infiltration became complex and preferential: the tensiometer C5 located at a depth of 20 cm reacted before the tensiometer D5 located at a depth of 17 cm. Moreover, the response time lag between tensiometers D1 and C6 located at the same depth (23 cm) was greater than 10 min (Figure 16).

[47] Figure 17 shows the evolution of the resistivity amplitude during the first infiltration-drainage cycle for the three frequencies, 93.7 Hz, 187 Hz, and 1.5 kHz. The results again validate the good sensitivity of resistivity to soil water content changes, i.e., the resistivity evolution reacted immediately when the rainfall rate was applied or stopped. They were also weakly frequency-dependent, as were the field measurements. Nevertheless, the results show two features that were not observed in the field: (1) a resistivity peak was recorded at time 20 min; (2) the resistivity began to increase at time 66 min during water infiltration, whereas the soil water content continued to increase.

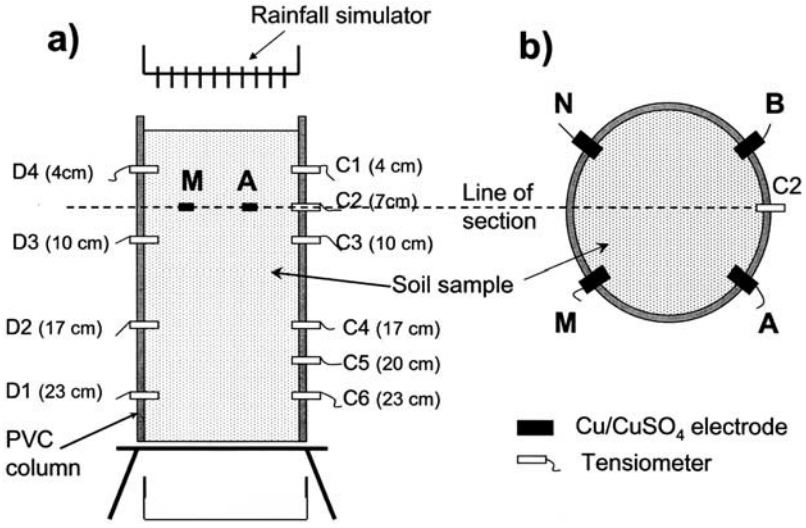

Figure 12. Schematic diagram of laboratory column in (a) section and (b) plan view (not to scale). Distance of tensiometer from soil surface is given in brackets.

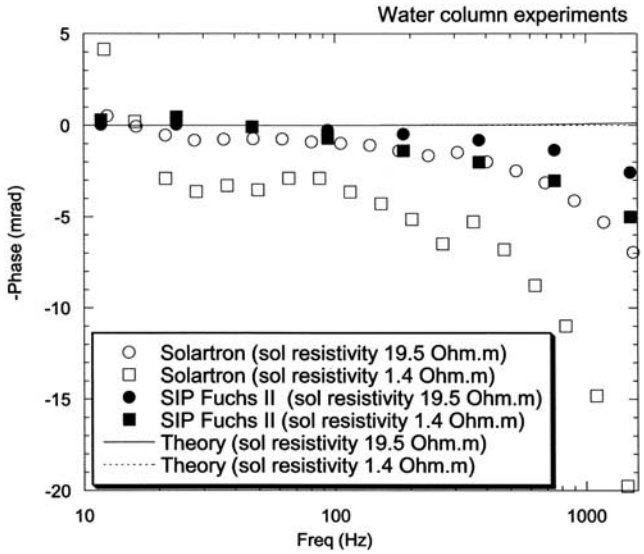

Figure 13. Positive phase errors measured on water samples by using both complex resistivity systems (Solartron and SIP-Fuchs) of this study.

[48] The first feature, i.e., the resistivity peak, is clearly associated with the arrival of the water front at the maximum sensitivity plane of the electrode array (see the C2 tensiometer evolution located at the same depth of 7 cm). It can be interpreted as a classical ''à-coup-de-prise'' which is usually observed in electrical investigations when a current electrode (A or B) is placed in contact with a highly resistive or conductive heterogeneity. This phenomenon is enhanced when high and shallow contrasts of resistivity exist at the soil surface. Moreover, it is interesting to note that a similar peak was observed in a rather different context during the migration of a hydrocarbon liquid through a porous medium within a laboratory column [*Chambers et al.*, 2004].

[49] The second feature (the increase of resistivity) is clearly related to the first arrival of water at the base of the column (Figure 17). Since resistivity is primarily a function of salinity and water content, the resistivity increase is here interpreted as a decrease in the salinity of the soil solution. As the infiltration process evolves, the percolating fresh water interacts geochemically with the solid and the initial water of the micropores, which is usually more concentrated [e.g., *Blackmore*, 1978]. As the seepage began at the base of the column and as fresh water was provided continually into the column, the pore water became more and more diluted by the fresh water. The EC of the retrieved water during the first 2 h of drainage was greater (1713 μS/cm) than the irrigation water (660 μS/cm).

[50] The phase evolution during the first infiltration-drainage cycle is shown for the three frequencies in Figure 18. The values of the tensiometer C2 located at the same depth (i.e., 7 cm) are also given in the same figure. In comparison with the field measurements, the laboratory results confirmed the rapid phase drop during the water infiltration. This phase drop, which is clearly associated with the water front past the plane of electrodes, is also frequency-dependent and is higher for the highest frequency ($\sim$15 mrad at 1.5 kHz). In order to estimate the impact of the phase errors observed on water samples (Figure 13), the phase measurements $\phi_{measured}$ were corrected using the following equation:

$$\phi_{corrected} = \phi_{measured} - \phi_{water\_samples} \tag{11}$$

where $\phi_{corrected}$ is the corrected phase; $\phi_{water\_samples}$ is the positive phase measured on water samples which would have the same resistivity value as the soil sample used in the column experiments. Since the positive phase errors were initially measured on water samples with only two resistivity values (1.4 Ohm·m and 19.5 Ohm·m), the $\phi_{water\_samples}$ values were extrapolated from these two values. The extrapolation was non linear (by using a power law) since (1) linear extrapolations gave negative error values and (2) a power law maximizes the error: it gives higher and thus safer values than the linear extrapolation. After correcting the phase measurements by using equation (11), a significant phase drop is still observed at 1.5 kHz (Figure 18). Moreover, as for the resistivity measurements, an inverse phase peak was also detected, which might have the same cause, i.e., an ''à-coup-de-prise''.

[51] However, contrary to the field experiment, an additional feature was present, i.e., the transient phase evolution was less noisy and erratic than that measured in the field. In our opinion, this feature seems to confirm the relationship between the electrical noise recorded for the phase measurements and the level of heterogeneity of the studied system. The good signal-to-noise ratio obtained in the laboratory is likely due to the location of the zone of the electrical maximum sensitivity in a homogenous part of the soil column, whereas the poor signal-to-noise ratio obtained in the field was mainly the consequence of preferential flow water in a heterogeneous soil at the scale of the electrical setup (see Figures 5a and 5b).

[52] Moreover, contrary to the field experiment, the phase did not increase when the rainfall stopped. This point can be explained by the relatively good homogeneity of the soil column in the plane of the measurement electrodes. Contrary to the field experiment where macropores with different sizes played a significant role, the soil involved in the column experiment was likely associated with much smaller

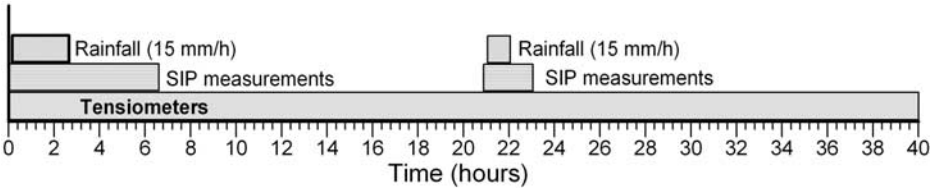

Figure 14. Schematic view of laboratory experimental procedure.

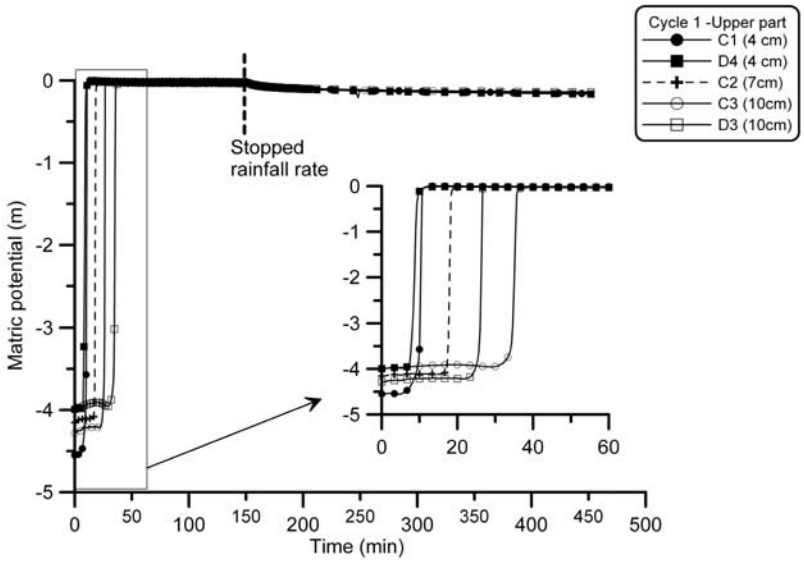

Figure 15. Tensiometer values at three depths (4 cm, 7 cm, and 10 cm) versus time (Cycle 1). At time 0, the rainfall rate was applied. The end of rainfall application is also indicated by a dashed line.

draining pores, which were still saturated when the rainfall stopped. On the other hand, in the field experiment, the numerous larger pores drained off rapidly as the rainfall ended. Consequently, as discussed hereafter, this comparison suggests that draining pore size is a key parameter in understanding the evolution of the measured polarizability.

[53] The resistivity amplitude and the phase measured during the second infiltration-drainage experiment are plotted in Figure 19 and Figure 20, respectively. As was the case during the first cycle, the evolution in resistivity amplitude exhibited the same transient signature with the same salinity effect during the water seepage at the base of the column. However, no resistivity peak was observed. This can be explained by a much lower contrast between the conductivity of the percolating water and that of the background. The pore water at the end of the first cycle was not necessarily in chemical equilibrium with the initial pore water in the soil aggregates: the water infiltration during the first cycle has not leached all the initial salts present in the soil.

[54] Similarly to the field experiment during Test 2, no significant phase drop was measured during the second infiltration-drainage cycle: the phase measurements were almost independent of the infiltration history of this cycle.

[55] In summary, the laboratory measurements confirmed the field observations: the SIP parameters, i.e., the resistivity amplitude and the phase, are saturation-dependent [e.g., *Ulrich and Slater*, 2004]. Moreover, the results validate the phase drop evidenced during water infiltration in the field in a dry soil. The existence of this phase drop does not depend on the electrode arrangement relative to the major direction of the water flow. At this stage, in order to use the SIP

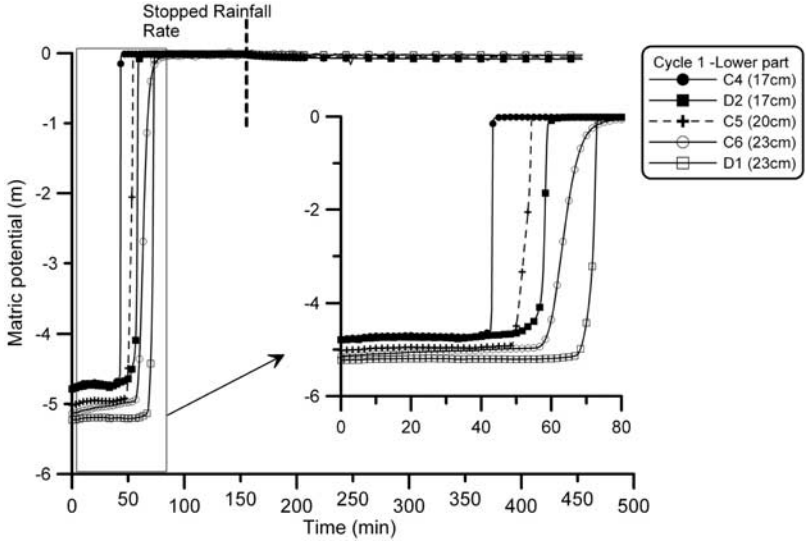

Figure 16. Tensiometer values at three depths (17 cm, 20 cm, and 23 cm) versus time (Cycle 1). At time 0, the rainfall rate was applied. The end of rainfall application is also indicated by a dashed line.

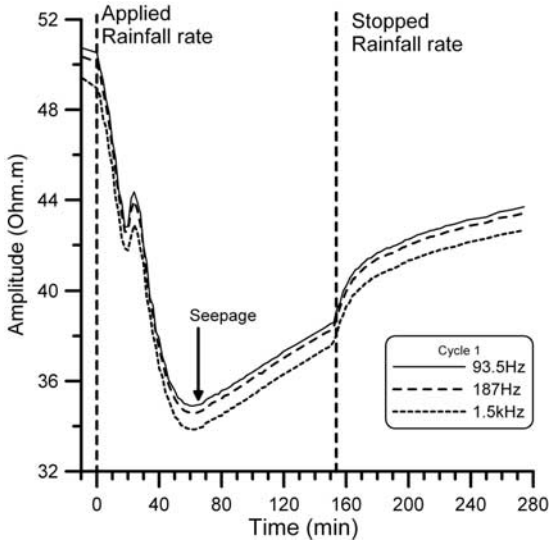

Figure 17. Resistivity amplitude spectra versus time (1st infiltration-drainage cycle). The beginning and the end of rainfall application are indicated by dashed lines. The time related to the seepage at the bottom of the column is indicated by an arrow.

approach for characterizing vertical flows in soils, it is necessary to provide some physical hypotheses to explain this new and original result. This is the main objective of the following section.

5. Discussion

[56] Our purpose in this section is not to provide a quantitative model of the field and laboratory experiments. There are at least two reasons for this. First, from a hydrological point of view, the results show that the vertical flows were complex and likely preferential in both cases. Moreover, many of the hydraulic parameters (hydraulic conductivity, distribution of the initial porosity and water content etc.) are unknown. Second, from a geophysical point of view, complex apparent resistivities were measured that are not intrinsic soil parameters: these apparent parameters depend on the electrode arrangement so a multielectrode system with a specific inversion model would be necessary in order to obtain a spatial distribution of the intrinsic parameters.

[57] The ensuing discussion focuses on the phase drop measured in both experimental studies, which showed the following features.

[58] ● The phase drop exists whatever the electrode arrangement (at least for the two configurations used in this study). It seems to be enhanced when the plane of the electrodes is perpendicular to the main direction of the water front.

[59] ● It occurs only if the soil is initially in a dry state, typically here with a matric potential lower than a few meters (Figures 6, 15 and 16). Indeed, both in the field and the laboratory, the following infiltration–drainage cycle did not exhibit any measurable phase drops.

[60] The second point suggests that, for this particular soil, a characteristic size of water-filled pores might exist, above which the phase drop vanishes. This characteristic size, r_c, can be bounded by two others, $r_{\min}$ and $r_{\max}$, which are respectively the smaller pore radius value estimated from the first infiltration-drainage cycle (exhibiting a phase drop) and the higher pore radius value estimated from the second infiltration-drainage cycles (with no phase drop).

$$r_{\min} < r_c < r_{\max}, \tag{12}$$

[61] Both bounds can be quantified from the Jurin equation [e.g., *Baver et al.*, 1972]:

$$r = \frac{2T\cos\gamma}{\rho_w g|h_i|} \tag{13}$$

where T is surface tension (= 0.075 N/m for an air-water interface), ρ_w is density of water, g is the gravitational acceleration, γ is the angle contact (taken equal to 0, in our case) and h_i is the matric potential measured prior to the application of the rainfall during the first infiltration-drainage cycle (to calculate $r_{\min}$) or during the second infiltration-drainage cycle (to calculate $r_{\max}$). To obtain the narrowest interval in the inequality (12), the tensiometer

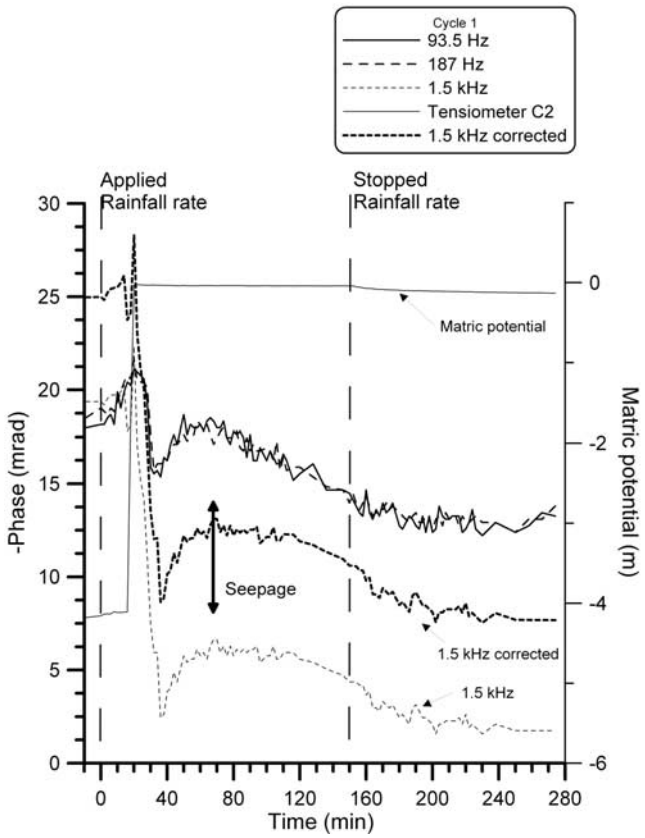

Figure 18. Phase spectra versus time (1st infiltration-drainage cycle). The values of the tensiometer located at the same depth (7 cm) are also given. C2 The beginning and the end of rainfall application are indicated by dashed lines. The time related to the seepage at the bottom of the column is indicated by an arrow. Typical error bars as a function of frequency are also given. The corrected phase values at 1.5 kHz are also shown. By convention the IP/capacitive effect is plotted as negative phase (i.e., -phase, $-\phi$).

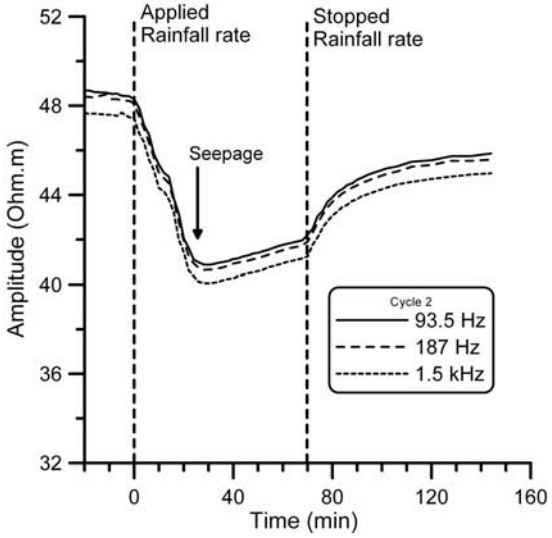

Figure 19. Resistivity amplitude spectra versus time (2nd infiltration-drainage cycle). The beginning and the end of rainfall application are indicated by dashed lines. The time related to the seepage at the bottom of the column is indicated by an arrow. For comparison, the same scale of amplitude used in Figure 17 has been used.

values from the field experiment were preferred to those from the laboratory experiments. In comparison with the column experiments, they provided a lower absolute value of the initial matric potential (i.e., a bigger pore radius), in the first infiltration-drainage cycle and a higher absolute value of the initial matric potential (i.e., a smaller pore radius) in the second infiltration-drainage cycle.

[62] By using equation (13) and the field results (Figures 6 and 9), the parameters $r_{\min}$ and $r_{\max}$ are respectively 14 μm ($h_i = -1.1$ m) and 43 μm ($h_i = -0.35$ m), respectively. Consequently, the corresponding pore diameter range is about [30–85 μm]

[63] An interesting point arises from this estimation: this estimated range can be referred to as the pore size of mesopores [30–75 μm], in accordance with the Soil Science Society of America's terminology (Table 2). Although the class limits given in Table 2 are necessarily somewhat arbitrary, this estimated range of [30–85 μm] also corresponds to the normally draining pores (or transmission pores) [*Greenland*, 1981; *Kay and Angers*, 2000] or to structural pores [*Stengel*, 1979]. Consequently, this statement strongly suggests that the measured phase drop is related to the transition of the water filling of mesopores or structural pores. In the following, the term "structural pores" is used since it covers a broader class of transmission draining pores (see Table 2).

[64] Nevertheless, at this stage, an important question remains: what is the physical origin of this phase drop that occurs as the water fills the structural pores? This question can also be reformulated by two others: Is the observed phase drop associated with a polarization mechanism? If so, among the different polarization mechanisms described previously, what is the relevant process?

[65] To answer these questions, it may be relevant to express our results in terms of complex permittivity or complex conductivity σ^*. As previously shown in experimental works [*Chelidze et al.*, 1999; *Slater and Glaser*, 2003; *Ulrich and Slater*, 2004], polarization magnitude is primarily included in the imaginary part σ'' (or in the real part κ'_{eff}) whereas the complex path of charge carriers in porous materials, i.e., charge transfer phenomena, is related to the real part σ' (or in the imaginary part κ''_{eff}). In other words, the complex resistivity ρ^* and especially the phase ϕ, are not direct measurements of polarization. In fact, as shown in equation (8), the phase ϕ almost defines the polarization magnitude relative to the conduction magnitude.

[66] Figures 21 and 22 show the evolution of the imaginary part σ'' and the real part σ' of the complex conductivity measured in the field and the laboratory for the 1.5 kHz frequency. Both figures confirm that the phase drop is clearly due to a decrease in the imaginary component σ'' i.e., a decrease in soil polarizability as the infiltrated water filled the structural pores.

[67] Since the phase drop is not related to the filling of micropores and is enhanced at high frequencies, it is safe to assume that the underlying polarization process associated with the phase drop is not purely electrochemical in relation with the EDL but rather a GI polarization. As far as a GI mechanism is concerned, the simplest depolarization effect related to the phase drop is a two-step process (Figure 23).

[68] 1. Before the arrival of the wetting front (stage 1 in Figure 23), water is mainly in the microporosity. The wet aggregates associated with the fine fraction of the soil generate a significant polarization magnitude whose physical origin is likely complex (i.e., combination of GI and EDL effect) and will not be discussed in detail here. Nevertheless, it is easy to imagine that during the application of an external electrical field, the interfaces between the wet aggregates and the interaggregate pores filled with air would constitute electrical barriers in which a significant

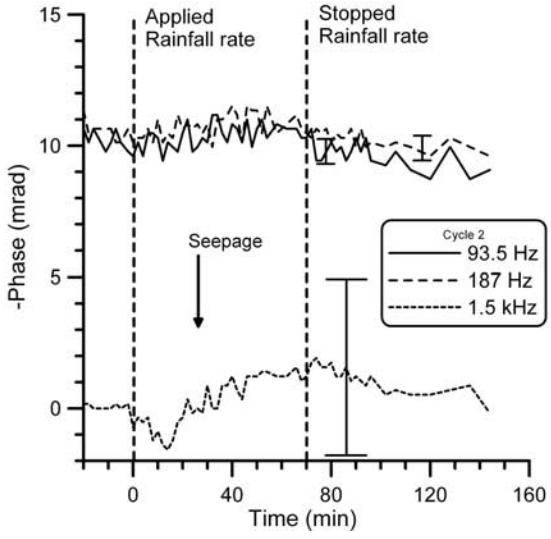

Figure 20. Phase spectra versus time (2nd infiltration-drainage cycle). The beginning and the end of rainfall application are indicated by dashed lines. The time related to the seepage at the bottom of the column is indicated by an arrow. Typical error bars as a function of frequency are also given. By convention the IP/capacitive effect is plotted as negative phase (i.e., −phase, $-\phi$).

Table 2. Pore Size Classification and Corresponding Functional Descriptions (*Soil Science Society of America*, 1997, From *Kay and Angers*, 2000; Modified From *Greenland*, 1981)

Class		Class limit (Equivalent Pore Diameter), μm	Functional Description	
Structural pores	Macropores	>75	normally draining pores	transmission pores
	Mesopores	30–75		
Micropores		5–30	slowly draining pores	
Ultramicropores		0.1–5	useful water retention capacity	storage pores
Cryptopores		<0.1	non useful water content	residual pores

amount of electrical charge carriers would be blocked, leading to the polarization of the wet aggregates.

[69] 2. The fresh water fills the structural pores bypassing the wet polarized aggregates, leading to a decrease in the bulk polarization amplitude (stage 2 in Figure 23). This process can be enhanced by the release of a large part of the charge carriers blocked in the aggregates by diffusion in the water-filled structural pores.

[70] It should be noted that this two-step process has got some similarities with the mechanism proposed by *Titov et al.* [2004] who studied the IP of unsaturated sands. They put in evidence a critical state, i.e., a critical saturation corresponding to the water filling of two different types of pores: large pores associated with bulk water and narrow pores related to adsorbed water films.

[71] In our case, the proposed Maxwell-Wagner effect (decrease in bulk polarizability due to filling of structural pores) can be illustrated by a simple calculation based on a MWHB model. We are aware that a simple MWHB model may not account for the very high soil heterogeneity. However as mentioned at the beginning of this section, our objective is not to propose a quantitative model that fits accurately all the data but to provide a physical hypothesis that explains the observed trends. For this purpose, this simple approach seems to be appropriate to capture the main physical processes at least in a first approximation.

[72] In this approach, the polarized wet aggregates composed of the soil fine fraction and the micropores (with possibly smaller pores) are modeled as oblate inclusions alternatively embedded in air (stage 1) and in fresh water (stage 2). The complex conductivity of the soil σ^* corresponding to both stages is calculated from equation (9) (MWHB model) expressed in complex conductivities:

$$\frac{\sigma^*_{ag} - \sigma^*}{\sigma^*_{ag} - \sigma^*_{a,w}} \left(\frac{\sigma^*_{a,w}}{\sigma^*} \right)^{1/m} = 1 - d_{ag} \qquad (14)$$

where d_{ag} is the volumetric fraction of aggregates; $\sigma^*_{a,w}$ is alternatively the complex conductivity of air (stage 1) or water (stage 2); σ^*_{ag} is the complex conductivity of the wet polarized aggregates that is considered as a fitting parameter since the polarization mechanisms related to the sole aggregates will not be discussed. As in *Samstag and Morgan* [1991], the imaginary part σ''_{ag} of the aggregates was estimated from the literature by assuming that the dielectric behavior of the aggregates with microporosity is similar in order of magnitude to that of a clay-rich rock with a very small structural porosity (i.e., argillite).

[73] The range of values of parameters $\sigma^*_{a,w}$ and σ^*_{ag} is given in Table 3. The results of a sensitivity analysis (not shown) demonstrated that a change in ±50 % of the σ''_{ag} value given in Table 3 has a low effect on the soil bulk imaginary conductivity. The particle shape factor (often called "cementation exponent") for all inclusions m in equation (13) is taken to be equal to 2 [e.g., *Rhoades et al.*, 1976; *Revil et al.*, 1998].

[74] A numerical application of this modeling approach is given in Figure 24 for two high frequencies, 1500 Hz and 150 Hz. Since the aggregates are filled with clay, the real conductivity of the aggregates has been chosen to be two-fold higher than the real conductivity of water. The volumetric fraction of wet aggregates has been chosen in the range of 60–90 % since the structural porosity is typically in the range 10–40 % in clay loamy soils [e.g., *Stengel*, 1979].

[75] The results in Figure 24 clearly show a drastic decrease in the soil imaginary conductivity between the two stages (before and after structural pore filling) for a frequency of 1.5 kHz. Compared to the experimental decrease, this calculated decrease is possibly overestimated by the underlying simplifications used in the model: in reality, from stage 1 to stage 2, charge carriers can also be transferred efficiently by diffusion in the water-filled structural pores and between aggregates, which may contribute

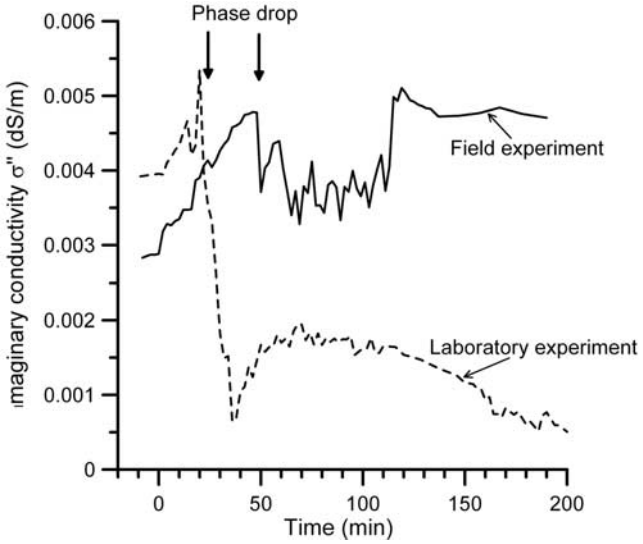

Figure 21. Imaginary conductivity versus time for field and laboratory experiments measured for a high frequency (1.5 kHz) (1st infiltration-drainage cycle). The times corresponding to the observed phase drop are indicated by arrows.

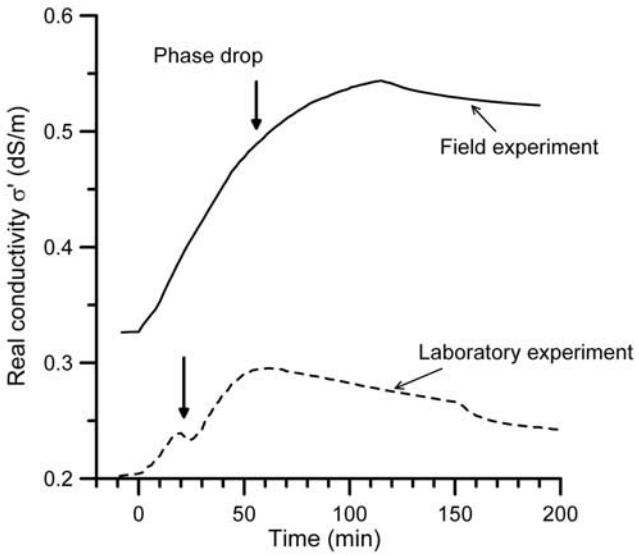

Figure 22. Real conductivity versus time for field and laboratory experiments measured for a high frequency (1.5 kHz) (1st infiltration-drainage cycle). The times corresponding to the observed phase drop are indicated by arrows.

to lowering the bulk polarizability. These aspects are not rigorously taken into account in the modeling process. Nevertheless, despite the uncertainties included in the calculations, this model is in agreement with the experimental trend; the drastic modeled decrease could explain quantitatively the phase drop observed in the field and in the laboratory.

[76] Moreover, one may wonder whether the MWHB equation is able to model the frequency dependence of the measured electrical properties. In other words, can this equation show that the observed phase drop is enhanced in the high part of the used frequency range? To answer this question, one has to introduce into the model a relationship between the electrical properties of aggregates and the frequency: indeed, there is no reason to suppose that the electrical properties of aggregates do not depend on frequency. Unfortunately, this relationship is unknown and is a priori difficult to obtain. However, a value of the relative dielectric permittivity of aggregates equal to 10^8 at 150 Hz (Table 3), which is not an unusual value for dense clayey rocks at low frequencies [e.g., *Comparon*, 2005; *Cosenza et al.*, 2007], leads to obtaining a lower phase drop compared to that calculated at 1500 Hz (Figure 24). Although this calculation is not a validation of the proposed model, it confirms the experimental trend i.e., the decrease in the observed phase drops with decreasing frequency. At this stage, we are aware that further experimental and theoretical investigations are required to fully validate this approach with regard to the frequency-dependent phenomena observed. In particular, we need to understand and to model the low frequency electrical spectra of highly clayey materials.

6. Conclusion

[77] In situ and laboratory experiments were undertaken to estimate the capabilities of the SIP method to characterize vertical flows in the vadose zone during water infiltration. These experimental investigations had two original features: (1) they were performed in the same silty clay loamy soil and (2) they coupled SIP and tensiometer measurements.

[78] During both experiments, the evolution in phase variation showed a significant drop at high frequencies (typically greater than 1 kHz) during the first infiltration

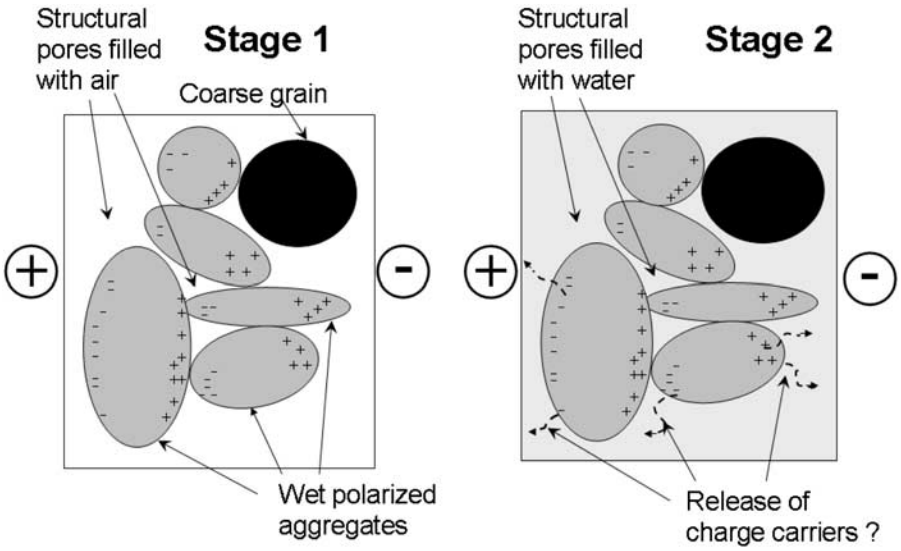

Figure 23. Schematic describing the two physical conditions (stages) related to the observed phase drop. The first stage corresponds to the condition before the arrival of the wetting front, in other words, before the water filling of the mesopores (pores typically greater than 30 μm). At this stage, water is located in the microporosity inside the polarized aggregates. Charge carriers are blocked in the aggregates since the air is electrically an isolator. The second stage represents the physical condition after the arrival of the wetting front: the mesopores are now filled with connected fresh water, leading to a decrease in the polarizability of the aggregates.

Table 3. Typical Range of Values for the Complex Electrical Conductivity of the Three Phases (Air, Water and Aggregates)[a]

Complex Electrical Conductivity	Range, S/m	References and Comments
Air		
$\sigma'_a = \sigma''_a = 0$		
Water		
σ'_w	$9.3\ 10^{-2}$	measured at 20°C
σ''_w	$7.\ 10^{-6}$ (f = 1500 Hz) $3.5\ 10^{-6}$ (f = 750 Hz)	The imaginary part σ''_w is calculated from the relative permittivity of water i.e., 80: $\sigma''_w = 2\pi \boldsymbol{f}\, \varepsilon_0\, 80$ where f is the frequency; ε_0 is the free space permittivity equal to $8.85\ 10^{-12}$ F/m.
Aggregates		
σ''_{ag}	$8.5\ 10^{-4}$ ($\varepsilon'_{ag} = 10^4$) (f = 1500 Hz)	The corresponding real relative dielectric permittivity is also given.
	$8.5\ 10^{-1}$ ($\varepsilon'_{ag} = 10^8$) (f = 150 Hz)	ε'_{ag} *Comparon* [2005], *Cosenza et al.* [2007]

[a]The parameters σ'_{ag} and σ''_{ag} are estimated from the literature by assuming that the dielectric behavior of the aggregates is similar to that of a clay-rich rock.

cycles. These phase drops were correlated to the water filling of pores whose equivalent diameters were estimated to be in the range of [30–85 μm]. This range might be related to structural porosity in this fine-grained soil.

[79] These phase drops were qualitatively and quantitatively interpreted as a GI mechanism, i.e., the decrease in polarization amplitude is mainly due to the filling of a conducting liquid in the structural pores between high polarized and wet aggregates.

[80] This work strongly suggests the need for further experimental and theoretical investigations in two directions. First, from a practical point of view, the SIP method seems to be able to monitor the filling of drainage pores and possibly in the field, thus providing indications about soil structural features. However, further field work is needed in different sites and other hydrological situations to validate this capability. Second, from a fundamental point of view, there is still no comprehensive understanding of the polarization mechanisms involved at the different pore scales (from micropores to macropores) so the SIP method cannot yet be used efficiently in the field. This is why theoretical investigations on the fundamental polarization mechanism that occurs in Earth materials must remain an active field of research.

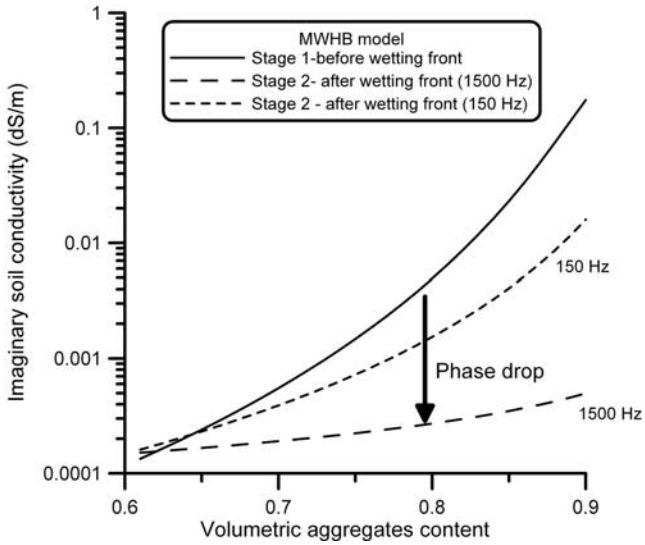

Figure 24. Calculated imaginary soil conductivity as a function of volumetric aggregate content. Both stages 1 and 2 (before and after the arrival of the wetting front) are considered.

[81] **Acknowledgments.** This research was supported by the Agence Nationale de la Recherche (ANR) –ECCO programs (POLARIS II Project: "Polarisation Provoquée Spectrale" – Spectral Induced Polarization and «Flux d'infiltration, recharge et hétérogénéité: une approche multiéchelle de la colonne à la parcelle» project n° 161 ACI ECCO 2003). We thank D. Slater, A. Kemna and two anonymous reviewers for their thoughtful comments that have significantly improved the initial manuscript.

References

Baver, L. D., W. H. Gardner, and W. R. Gardner (1972), *Soil Physics*, John Wiley, New York.

Binley, A., and A. Kemna (2005), DC resistivity and Induced Polarization methods, in *Hydrogeophyisics*, edited by Y. Rubin and S. Hubbard, pp. 129–156, Springer-Verlag, Berlin Heidelberg, Germany.

Binley, A., L. D. Slater, M. Fukes, and G. Cassiani (2005), Relationship between spectral induced polarization and hydraulic properties of saturated and unsaturated sandstone, *Water Resour. Res.*, *41*, W12417, doi:10.1029/2005WR004202.

Blackmore, A. V. (1978), Interpretation of electrical conductivity in a clay soil containing salts, *Aust. J. Soil Res.*, *16*, 311–318.

Börner, F. D. (2006), Complex conductivity measurement, in *Groundwater Geophysics-A Tool for Hydrogeology*, edited by R. Kirsh, pp. 119–153, Springer, Berlin, Germany.

Börner, F. D., and J. H. Schön (1991), A relation between the quadrature component of electrical conductivity and the specific surface area of sedimentary rocks, *Log Anal.*, *32*, 612–613.

Börner, F. D., W. Schopper, and A. Weller (1996), Evaluation of transport and storage properties in the soils and groundwater zone from induced polarization measurements, *Geophys. Prospect.*, *44*, 583–601.

Bouyoucos, G. J., and A. H. Mick (1940), An electrical resistance method for the continuous measurement of soil moisture under field conditions, *MI Agric. Exp. Sta. Tech. Bull.*, *172*, 1–38.

Chambers, J. E., M. H. Loke, R. D. Ogilvy, and P. I. Meldrum (2004), Noninvasive monitoring of DNAPL migration through a saturated porous medium using electrical impedance tomography, *J. Contam. Hydrol.*, *68*, 1–22.

Chanzy, A., A. Tarussov, A. Judge, and F. Bonn (1996), Soil water content determination using a digital ground-penetrating radar, *Soil. Sci. Soc. Am. J.*, *60*, 1318–1326.

Chelidze, T. L., and Y. Guéguen (1999), Electrical Spectroscopy of Porous Rocks: A review – I. Theoretical models, *Geophys. J. Int.*, *137*, 1–15.

Chelidze, T., Y. Guéguen, and C. Ruffet (1999), Electrical spectroscopy of porous rocks: A review – II. Experimental results and interpretation, *Geophys. J. Int.*, *137*, 16–34.

Comas, X., and L. Slater (2004), Low-frequency electrical properties of peat, *Water Resour. Res.*, *40*, W12414, doi:10.1029/2004WR003534.

Comparon, L. (2005) Etude expérimentale des propriétés électriques et diélectriques des matériaux argileux, Ph.D. thesis, Institut de Physique du Globe, Paris, France.

Cosenza, Ph., C. Camerlynck, and A. Tabbagh (2003), Differential effective medium schemes for investigating the relationship between high-frequency relative permittivity and water content of soils, *Water Resour. Res.*, *39*(9), 1230, doi:10.1029/2002WR001774.

Cosenza, Ph., A. Ghorbani, N. Florsch, and A. Revil (2007), Effects of drying on the low-frequency electrical properties of Tournemire agillites, *Pure Appl. Geophys.*, *164*, 1–24, doi:10.1007/s00024-007-0253-0.

Daily, W. D., A. L. Ramirez, D. J. LaBrecque, and J. Nitao (1992), Electrical resistivity tomography of vadose water movement, *Water Resour. Res.*, *28*, 1429–1442.

Davis, J. L., G. C. Topp, and P. Annan (1977), Measuring soil water content in-situ using time domain reflectometry techniques, in *Current Research, Part B*, pp. 33–36, Geol. Surv. of Canada, Paper 77-IB.

Dingman, L. (2002), *Physical Hydrology*, 2nd ed., 646 pp., Prentice Hall, Upper Saddle River, N. J.

Edwards, L. S. (1977), A modified pseudosection for resistivity and IP, *Geophysics*, *42*(5), 1020–1036.

Greenland, D. J. (1981), Soil management and soil degradation, *J. Soil Sci.*, *32*, 301–332.

Guéguen, Y., and V. Palciauskas (1994), *Introduction to the Physics of Rocks*, Princeton Univ. Press, Princeton, N. J.

Hagrey, S. A., and J. Michaelsen (1999), Resistivity and percolation study of preferential flow in vadose zone at Bokhorst, Germany, *Geophysics*, *64*(3), 746–753.

Ingeman-Nielsen, T., and F. Baumgartner (2006), CR1mod, a Mathlab program to model 1D complex resistivity effects in electrical and electromagnetic surveys, *Comput. Geosci.*, *32*(9), 1411–1419.

Kay, B. D., and D. A. Angers (2000), Soil structure, in *Handbook of Soil Science*, edited by M. E. Sumner, pp. 229–276, CRC Press, Boca Raton, USA.

Keller, G. V., and F. C. Frischknecht (1982), *Electrical Methods in Geophysical Prospecting*, Elsevier, Oxford.

Lesmes, D. P., and F. D. Morgan (2001), Dielectric spectroscopy of sedimentary rocks, *J. Geophys. Res*, *106*(B7), 13,329–13,346.

Lima, O. A. L., and S. Niwas (2000), Estimation of hydraulic parameters of shaly sandstone aquifers from geoelectrical measurements, *J. Hydrol.*, *235*, 12–26.

Lyklema, J. (1995), *Fundamentals of Interface and Colloid Science*, Elsevier, London, U.K.

Marshall, D. J., and T. R. Madden (1959), Induced Polarization: A study of its Causes, *Geophysics*, *24*, 790–816.

Maxwell, J. C. (1891), *Treatise on Electricity and Magnetism*, vol. 2, 2nd ed., Clarendon, Oxford.

Olhoeft, G. (1985), Low-frequency electrical properties, *Geophysics*, *50*, 2492–2503.

Parasnis, D. S. (1997), *Principles of Applied Geophysics*, CRC Press, London.

Petiau, G. (2000), Second generation of Lead-Lead Chloride electrodes for geophysical applications, *Pure Appl. Geophys.*, *157*, 357–382.

Revil, A., L. M. Cathles III, S. Losh, and J. A. Nunn (1998), Electrical conductivity in shaly sands with geophysical applications, *J. Geophys. Res.*, *103*(B3), 925–936.

Rhoades, J. D., P. A. C. Raats, and R. J. Prather (1976), Effects of liquid-phase electrical conductivity, water content, and surface conductivity on bulk soil electrical conductivity, *Soil Sci. Soc. Am. J.*, *40*, 651–655.

Samstag, F. J., and F. D. Morgan (1991), Induced Polarization of shaly sands: Salinity domain modeling by double embedding of the effective medium theory, *Geophysics*, *56*(11), 1749–1756.

Santamarina, J. C. (2001), *Soils and Waves*, John Wiley, New York.

Scott, J. B. T., and R. D. Barker (2003), Determining pore-throat size in Permio-Triassic sandstones from low-frequency electrical spectroscopy, *Geophys. Res. Lett.*, *30*(9), 1450, doi:10.1029/2003GL016951.

Slater, L., and D. R. Glaser (2003), Controls on induced polarization in sandy unconsolidated sediments and application to aquifer characterization, *Geophysics*, *68*(5), 1547–1588, doi:10.1190/1.1620628.

Slater, L., D. Ntarlagiannis, and D. Wishart (2005), On the relationship between induced polarization and surface area in metal-sand and clay-sand mixtures, *Geophysics*, *71*(2), A1–A5, doi:10.1190/1.2187707.

Smith-Rose, R. L. (1933), The electrical properties of soils for alternating currents at radiofrequencies, *Proc. R. Soc., Ser. A and Ser. B.*, *140*, 359.

Soil Science Society of America (1997), *Glossary of Soil Science Terms*, Soil Sci. Soc. of Am., Madison.

Stengel, P. (1979), Utilisation des systèmes de porosité pour la caractérisation de l'état physique du sol in in situ, *Ann. Agron.*, *30*(1), 27–51.

Tabbagh, A., M. Dabas, A. Hesse, and C. Panissot (2000), Soil resistivity: A non-invasive tool to map soil structure horizonation, *Geoderma*, *97*, 393–404.

Titov, K., V. Komarov, V. Tarasov, and A. Levitski (2002), Theoretical and experimental study of time-domain-induced polarization in water saturated sands, *J. Appl. Geophys.*, *50*(4), 417–433.

Titov, K., A. Kemna, A. Tarasov, and H. Vereecken (2004), Induced polarization of unsaturated sands determined through time domain measurements, *Vadose Zone J.*, *3*, 1160–1168.

Tong, M., L. Li, W. Wang, and Y. Jiang (2006), Determining capillary-pressure curve, pore-size distribution, and permeability from induced polarization of shaley sand, *Geophysics*, *71*(3), N33–N40, doi:10.1190/1.2195989.

Tran Ngoc, Lan, P. Chaigneand A. Philippe (1972), Expérimentation d'une méthode capacitive pour l'évolution de l'humidité des sols, *Bull. liaison Lab. Ponts Chaussées*, *60*, 155–165.

Ulrich, C., and L. Slater (2004), Induced polarization measurements on unsaturated, unconsolidated sands, *Geophysics*, *69*(3), 762–771.

Van Voorhis, G. D., P. H. Nelson, and T. L. Drake (1973), Complex resistivity spectra of porphyry cooper mineralization, *Geophysics*, *38*, 49–60.

Vinegar, H. J., and M. H. Waxman (1984), Induced polarization of shaly sands, *Geophysics*, *49*(9), 1267–1287.

Wagner, K. W. (1924), Erklarung der Dielectrishen Nachwirkungsvorgange auf grund Maxwellscher vorstellungen, *Arch. Electrotech.*, *2*, 371–381.

Ward, S. H. (1990), Resistivity and induced polarization methods, in *Geotechnical and Environmental Geophysics*, edited by S. T. Ward, vol. I, *Review and Tutorial*, Soc. of Explor. Geophys., Tulsa, Oklahoma.

Zhou, Q. Y., J. Shimada, and A. Sato (2001), Three-dimensional spatial and temporal monitoring of soil water content using electrical resistivity tomography, *Water Resour. Res.*, *37*(2), 273–285.

Ph. Cosenza, N. Florsch, and A. Ghorbani, UPMC, University of Paris 06, UMR 7619 Sisyphe, Case Courrier 105, 4 Place Jussieu, Paris 75252, France. (cosenza@ccr.jussieu.fr)

C. Doussan and S. Ruy, INRA-UMR Climat, Sol et Environnement Domaine St. Paul - Agroparc, 84 914 Avignon Cedex 9, France.